

Magnetic-field-induced photoluminescence enhancement in type-I quantum wells: A quantitative probe for interface flatness

Jun Shao(邵军), Man Wang(王嫚), Xiren Chen(陈熙仁), Liangqing Zhu(朱亮清), F. X. Zha(查访星), H. Zhao, Shumin Wang(王庶民), and Wei Lu(陆卫)

Citation: Chin. Phys. B, 2025, 34 (**10**): 107802. DOI: 10.1088/1674-1056/adf5a7
http://cpb.iphy.ac.cn; http://iopscience.iop.org/cpb

What follows is a list of articles you may be interested in

Layer-dependent exciton dynamics in InSe/WS_2 heterostructures

Siyao Li(李思垚), Yufan Wang(王雨凡), Zhiqiang Ming(明志强), Yong Liu(刘勇), Lanyu Huang(黄岚雨), Siman Liu(刘思嫚), Jialong Li(李佳龙), Yulin Chen(成昱霖), Zhoujuan Xu(徐周娟), Zeyu Liu(刘泽宇), Danliang Zhang(张丹亮), and Xiao Wang(王笑)

Chin. Phys. B, 2025, 34 (**9**): 097802. DOI: 10.1088/1674-1056/adc6f7

Effects of helium ion irradiation and thermal annealing on the optical and structural properties of hexagonal boron nitride

Guan-Lin Liu(刘冠麟), Ji-Lian Xu(徐辑廉), Peng-Tao Jing(景鹏涛), Jing-Jing Shao(邵京京), Xu Guo(郭旭), Yun-Tao Wu(吴韵涛), Feng Qin(覃凤), Zhen Cheng(程祯), Deming Liu(刘德明), Yang Bao(鲍洋), Hai Xu(徐海), Li-Gong Zhang(张立功), Da Zhan(詹达), Jia-Xu Yan(闫家旭), Lei Liu(刘雷), and De-Zhen Shen(申德振)

Chin. Phys. B, 2025, 34 (**5**): 057801. DOI: 10.1088/1674-1056/adbee7

Temperature-dependent photoluminescence of lead-free cesium tin halide perovskite microplates

Jiayu Tan(谭佳雨), Yixuan Zhou(周译玄), De Lu(卢德), Xukun Feng(冯旭坤), Yuqi Liu(刘玉琪), Mengen Zhang(张蒙恩), Fangzhengyi Lu(卢方正一), Yuanyuan Huang(黄媛媛), and Xinlong Xu(徐新龙)

Chin. Phys. B, 2023, 32 (**11**): 117802. DOI: 10.1088/1674-1056/ad028e

Anomalous photoluminescence enhancement and resonance charge transfer in type-II 2D lateral heterostructures

Chun-Yan Zhao(赵春艳), Sha-Sha Li(李莎莎), and Yong Yan(闫勇)

Chin. Phys. B, 2023, 32 (**8**): 087801. DOI: 10.1088/1674-1056/acc1d1

Enhanced photoluminescence of monolayer MoS_2 on stepped gold structure

Yu-Chun Liu(刘玉春), Xin Tan(谭欣), Tian-Ci Shen(沈天赐), and Fu-Xing Gu(谷付星)

Chin. Phys. B, 2022, 31 (**8**): 087803. DOI: 10.1088/1674-1056/ac657b

---

RAPID COMMUNICATION

Magnetic-field-induced photoluminescence enhancement in type-I quantum wells: A quantitative probe for interface flatness

Jun Shao(邵军)[1,2,†], Man Wang(王嫚)[1,3], Xiren Chen(陈熙仁)[4,5,‡], Liangqing Zhu(朱亮清)[6], F. X. Zha(查访星)[7], H. Zhao[8], Shumin Wang(王庶民)[8,§], and Wei Lu(陆卫)[1,2]

[1] *State Key Laboratory for Infrared Physics, Shanghai Institute of Technical Physics, Chinese Academy of Sciences, Shanghai* 200083, *China*
[2] *Hangzhou Institute for Advanced Study, University of Chinese Academy of Sciences, Hangzhou* 310024, *China*
[3] *University of Chinese Academy of Sciences, Beijing* 100049, *China*
[4] *National Key Laboratory of Infrared Detection Technologies, Shanghai Institute of Technical Physics, Chinese Academy of Sciences, Shanghai* 200083, *China*
[5] *Key Laboratory of Infrared Imaging Materials and Detectors, Shanghai Institute of Technical Physics, Chinese Academy of Sciences, Shanghai* 200083, *China*
[6] *Key Laboratory of Polar Materials and Devices, Ministry of Education, East China Normal University, Shanghai* 200062, *China*
[7] *Physics Department, Shanghai University, Shanghai* 200444, *China*
[8] *Department of Microtechnology and Nanoscience, Chalmers University of Technology, S*-41296 *Göteborg, Sweden*

(Received 17 June 2025; revised manuscript received 11 July 2025; accepted manuscript online 30 July 2025)

Interfacial disorders in semiconductor quantum wells (QWs) determine material properties and device performance and have attracted great research efforts using different experimental methods. However, so far, there has been no way to quantify the lateral length distribution of the interfacial disorders in QWs. Since photoluminescence (PL) is sensitive to exciton localization, the evolutions of PL energy and linewidth under external perpendicular magnetic fields have served as effective measurement methods for QW analysis; however, the evolution of PL intensity has not played a matching role. In this paper, we develop a theoretical model correlating the PL intensity with the interfacial disorders of type-I QWs under an external perpendicular magnetic field. We verify the model's rationality and functionality using InGa(N)As/GaAs single QWs. In addition, we derive the Urbach energy and determine the lateral length distribution of interfacial disorders. The results show that the magnetic field-dependent PL intensity, as described by our model, serves as a valid probe for quantifying the interface flatness. The model also reveals that the mechanism of magnetic-field-induced intensity enhancement is a joint effect of interfacial disorder-induced exciton localization and the transfer of excitons from dark to bright states. These insights may benefit performance improvements of type-I QW materials and devices.

Keywords: photoluminescence, type-I quantum wells, interfacial disorders, magnetic field

PACS: 78.55.–m, 78.67.De, 79.60.–i, 79.60.Jv

DOI: 10.1088/1674-1056/adf5a7 **CSTR:** 32038.14.CPB.adf5a7

1. Introduction

Interfacial disorders inevitably occur in epitaxially grown semiconductor quantum well (QW) structures due to well-width variations on different lateral length scales at the monolayer (ML) level. Such disorders lead to exciton localization in the potential minima associated with regions of enhanced well thickness.[1] Interfacial disorders are a key factor in determining the properties of QWs[2] and impact the performance of optoelectronic devices such as laser diodes,[3] quantum-cascade detectors,[4] light-emitting diodes (LEDs),[5] and quantum-cascade lasers (QCLs).[6] Taking the exciton Bohr radius as a measure of lateral confinement, three statistical disorders have been defined: those at the atomic scale, those at the length scale of the exciton Bohr radius, and those at the long-range scale.[7] To characterize interfacial disorders, different techniques have been employed, e.g., x-ray scattering, cross-sectional scanning tunneling microscopy (XSTM), atomic force microscopy (AFM), transport measurement, and photoluminescence (PL) spectroscopy. X-ray scattering measures interfacial disorders in the growth direction on an atomic scale. It has revealed that the distributions of As and Ga atoms in the growth direction are about 2.7 and 1.6 MLs, respectively, in InGaAs/InP QWs, though it did not detect step-like interfacial disorders in the lateral direction.[8] XSTM reveals interfacial disorder on an atomic scale in both the growth and lateral directions. It identified that the As composition profile in InGaAs/InP QWs has an exponential variation in the growth direction and observed a reduction in the disorder amplitude to 0.45 nm and an increase in the lateral length to 27 nm due to a growth interruption of 30 s.[9] AFM has been used to ob-

†Corresponding author. E-mail: jshao@mail.sitp.ac.cn
‡Corresponding author. E-mail: xrchen@mail.sitp.ac.cn
§Corresponding author. E-mail: shumin@chalmers.se

© 2025 Chinese Physical Society and IOP Publishing Ltd. All rights, including for text and data mining, AI training, and similar technologies, are reserved.

serve interfacial disorders of ML islands with different sizes. It revealed ordered steps with height variations of more than 1 ML separated by about 75 nm in GaAs/AlGaAs QWs.[10] Transport measurement correlates interfacial disorders with carrier mobility. It has been used to characterize interfacial disorders by the height δ and the length ξ of Gaussian-like fluctuations[11] and determined these dimensions to be 0.6 nm and 63 nm, respectively, in InGaAs/InP superlattices (SLs).[12] Nevertheless, so far, we do not have a quantitative method that can statistically assess the lateral length distribution of interfacial disorders (also referred to as interface flatness) on the millimeter scale in QWs.

PL spectroscopy provides abundant information about crystalline quality and electronic structures [13–21] and has found wide application, particularly when its functionality was extended to wide infrared and micrometer-scale spatially resolved scanning imaging.[22–28] Photoluminescence studies have shown that, at low temperatures, excitons are predominantly localized. For example, in (Al,Ga)As/GaAs QWs, this localization occurs due to fluctuations in the effective QW thickness;[29] in GaAs/AlGaAs QWs, it results from interface fluctuations on different length scales[30] or short-range correlated interface disorder;[7] in CdTe/CdMnTe QWs, it is caused by the heterointerface;[31] and in AlInAsSb digital alloys, by the InSb interface layer.[32] As an advanced PL technique, magneto-PL spectroscopy is based on the manipulation of PL properties by external magnetic fields. Excitons in QWs undergo a diamagnetic shift and in-plane shrinkage under a perpendicular magnetic field.[33] Among several techniques, such as temperature-dependent PL, PL energy as a function of magnetic field provides the most information about exciton binding energy E_b and reduced effective mass μ in QWs,[34] with the aid of standard effective-mass theory for quasi-two-dimensional magneto-excitons.[34] The PL linewidth has been used to probe the length scales of interfacial disorders in QWs, and the observations of either a monotonically increasing or field-dependent decreasing linewidth in GaAs/AlGaAs QWs and InAs/GaSb SLs have been explained by postulating the existence of two lateral-length interfacial disorders.[35,36] The PL intensity has also attracted interest, and intensity enhancements have been observed in GaAs/AlGaAs QWs,[37] which are considered to be the result of localization and/or interfacial disorder effects. Similarly, magnetic-field enhancement of lasing emission has been observed in GaAs/$Al_{0.15}Ga_{0.85}As$ devices and InGaAs/GaAsSb terahertz QCLs[38,39] and has been recognized as a major impact of interface roughness scattering. Nevertheless, to date, we do not have a model that fits PL intensity and quantifies the distribution of interfacial disorders.

In this study, a theoretical model is developed for the magnetic-field-dependent PL intensity of type-I QWs in an external perpendicular magnetic field, based on basic assumptions about interfacial disorders caused by Gaussian-distributed fluctuations in well thickness and magnetic-field-induced transfer of dark excitons with a nonzero center-of-mass (COM) momentum K around $K = 0$ to bright states. For verification, three as-grown and rapid thermally annealed (RTA) InGa(N)As/GaAs single QW (SQW) samples are employed. The amplitude distribution of interfacial disorders caused by fluctuations in the well-layer thickness is checked by excitation-power-dependent PL measurements. The Urbach energy and the lateral-length distribution of the interfacial disorders are derived from magnetic-field-dependent PL experiments and compared to the values available in the literature, and the mechanism of the PL intensity enhancement and the interfacial effects of N incorporation and rapid thermal annealing are discussed. We draw the conclusion that the PL enhancement originates from the field-induced transfer of excitons from dark states to bright states and that our model can serve as an effective probe for quantifying the Urbach energy and lateral-length distribution of the interfacial disorders in type-I QWs.

2. Theoretical model

The motion of quasi-two-dimensional excitons in QWs can be described in terms of uncorrelated relative and COM motions. In conventional nonresonant-excitation PL measurements, a pumping light (generally, a laser) is employed that has a higher energy than the fundamental bandgap. The pumping light excites valence-band electrons into the conduction band and leaves holes behind. The electron–hole pairs relax, first forming excitons with large COM momenta via scattering with acoustic phonons,[40] and then losing momentum via exciton–exciton collisions to reach states where radiative recombination may take place.[41] The excitons are unstable; some recombine by emitting photons (and contributing to PL) and are known as bright-state excitons. Others are forbidden from radiating by selection rules due to their nonzero in-plane COM momentum ($K \neq 0$)[42] or total angular momentum $J = 2$[43] and are known as dark-state excitons. It has been shown that an external magnetic field applied in the plane of the QW can tailor the radiative properties of excitons in GaAs/AlGaAs coupled QWs by coupling the relative and COM motions, shifting the ground state of the excitons from $K = 0$ to states with finite $K \neq 0$ and transferring the excitons from bright to dark states.[44] In this study, the effect of an external magnetic field perpendicular to the QW plane is considered, and an inverse exciton transfer from dark to bright states is demonstrated.

For a QW in a magnetic field (B) perpendicular to the QW plane, the magnetic-field effect on exciton wave functions depends on $\zeta = e\hbar B/(2\mu E_b)$: (i) in a low field of

$\zeta \ll 1$, the wave functions hardly change; (ii) in a high-field limit of $\zeta \gg 1$, electrons and holes undergo cyclotron motion, and perturbation from Coulomb interaction generates Landau states; and (iii) in a medium field of $\zeta \approx 1$, which corresponds to about 4–6 T for InGa(N)As/GaAs QWs,[45] an effective-mass equation for quasi-two-dimensional magneto-exciton treats the Coulomb potential and the magnetic-field energy in a balanced way,[34]

$$\begin{aligned}&\left\{-\frac{\hbar^2}{2\mu}\left[\frac{1}{\rho}\frac{\partial}{\partial\rho}\left(\rho\frac{\partial}{\partial\rho}\right)-\frac{m^2}{\rho^2}\right]+\frac{e^2}{8\mu}B^2\rho^2+V(\rho)\right.\\&\left.+\frac{e}{2}\left[\frac{1}{m^*_{\mathrm{h},\rho}}-\frac{1}{m^*_{\mathrm{e},\rho}}\right]Bm\hbar\right\}R_{n,m}(\rho)\\&=E_{\mathrm{r}}R_{n,m}(\rho),\end{aligned}$$

$$V(\rho)=\frac{-e^2}{4\pi\varepsilon_0}\int_{-\infty}^{+\infty}\int\frac{|Z_{\mathrm{e}}(z_{\mathrm{e}})|^2\,|Z_{\mathrm{h}}(z_{\mathrm{h}})|^2}{\varepsilon_{\mathrm{r}}(z_{\mathrm{e}},z_{\mathrm{h}})\sqrt{\rho^2+(z_{\mathrm{e}}-z_{\mathrm{h}})^2}}\,\mathrm{d}z_{\mathrm{e}}\,\mathrm{d}z_{\mathrm{h}},\quad(1)$$

where ρ is the in-plane distance between the electron and hole of the exciton pair; $m^*_{\mathrm{e},\rho}$ and $m^*_{\mathrm{h},\rho}$ are the in-plane effective masses of electrons and holes in the QW layer, respectively; m is the angular momentum quantum number; $m=0$ corresponds to S-type and $m=\pm1,\pm2$ correspond to P- and D-type exciton states, respectively; $Z_{\mathrm{e}}(z_{\mathrm{e}})$ and $Z_{\mathrm{h}}(z_{\mathrm{h}})$ are the confined-state wave functions of electrons and holes, respectively; $\varepsilon_{\mathrm{r}}\varepsilon_0$ is the dielectric constant of the well or the barrier, depending on z_{e} and z_{h}; and $R_{n,m}(\rho)$ is the excitonic envelope function. Numerical solutions and fitting to the experimental diamagnetic shift allow us to derive E_{b}, μ, and the zero-field exciton Bohr radius $a_{\mathrm{B}}=4\pi\varepsilon_0\varepsilon_{\mathrm{r}}\hbar^2/(\mu e^2)$. Here, the effects of spin-splitting and the P- and D-states are ignored, as they are not detectable under low to medium fields.[37]

The interfacial disorders that occur in QWs are introduced by the fluctuations of well-layer thickness and/or alloy composition and can be described by a phenomenological interface model, as shown in Fig. 1(a).[30] The rough bottom and top interfaces are equivalent to the combination of a smooth bottom interface and a rough top interface with disorders of average, wider, and narrower well-layer thicknesses of L_0, $L_0+\delta$, and $L_0-\delta$, respectively; L_0 is the mean thickness of the well layer, and δ is the amplitude of the thickness fluctuation. A region of the QW where the well layer is thicker, encircled by barriers, forms a lateral perturbation potential and may act as a trap that localizes excitons with $D_{\mathrm{ex}}\le\xi$, as illustrated by the (red) circled D_{ex}. The lateral length follows a Gaussian distribution, as indicated in Refs. [11,12], which will be confirmed by excitation power- and magnetic-field-dependent PL analyses. Here, ξ can be described by

$$g_{\mathrm{ex}}(\xi)\sim\mathrm{e}^{-\xi^2/2w^2},\quad(2)$$

as depicted in Fig. 1(b), where the focus $\bar{\xi}$, i.e., the mean lateral length of interfacial disorders, is at the zero point of the abscissa for convenience; w^2 is the variance; and $2\sqrt{2\ln 2}w$ is the full-width at half-maximum (FWHM) of the Gaussian distribution. As is shown shortly, it can be seen that setting the focus $\bar{\xi}$ at zero affects neither the formula derivation nor the estimation of the mean lateral length of the interfacial disorders. In principle, all the interfacial disorders with well-layer thicknesses $L\ge(L_0-\delta)$ may serve as traps that localize excitons. The lateral perturbation potential is considered to mainly affect the COM motion of excitons and to lead to the coupling of the COM motion to the relative motion.[7]

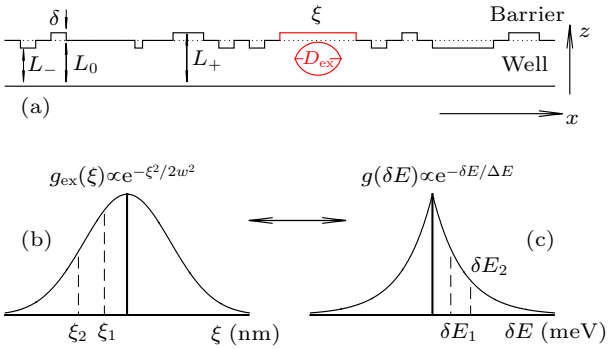


Fig. 1. (a) Interfacial disorders in QWs. L_0, L_+, and L_- denote the average, wider, and narrower well-layer thicknesses; δ denotes the amplitude of the thickness fluctuation. The circled D_{ex} represents an exciton trapped by a lateral perturbation potential with well-layer thickness of L_+ and a lateral length of $\xi\ge D_{\mathrm{ex}}$. (b) Real-space lateral-length Gaussian distribution of interfacial disorders, and (c) the corresponding lateral perturbation potential density of states.

The energy eigenvalue of the lateral perturbation potential, δE, can be approximated by a finite-depth square-well model with a lateral length of ξ as the well width,[46] $\delta E=\hbar^2k_{\parallel}^2/2\mu$, where $k_{\parallel}$ is the in-plane wave vector along the interface. This approach, together with the Fourier transform of the real-space Gaussian distribution [Eq. (2)] to the k space,[47] results in (following the Urbach rule[48]) an exponential density of states, as illustrated in Fig. 1(c):

$$g(\delta E)\sim\mathrm{e}^{-\delta E/\Delta E},\quad\Delta E=\frac{\hbar^2}{\mu w^2},\quad(3)$$

with a focus at zero. Here, ΔE is the interfacial Urbach energy quantifying the potential energy fluctuation of the interfacial disorders. Urbach energy, as the key parameter of Urbach rule, defines the exponential band tail states arising from the Gaussian distribution of the local potential wells[49] or compositional and structural inhomogeneities.[50] Urbach energy has attracted significant research effort,[47,51] mainly based on PL at different temperatures and excitation powers,[52] due to its importance in solar energy conversion,[53,54] LED applications,[55] and photoluminescent upconversion.[56] To date, however, we have not seen a magneto-PL description of the interfacial Urbach energy in QWs.

In a zero magnetic field, interfacial disorders with $\xi\ge D_{\mathrm{ex}}$ localize, by an additional energy δE, excitons with COM momenta $K=0$ and slightly deviating from $K=0$. In nonzero low-to-medium ($0\le\zeta\approx1$) magnetic fields, excitons undergo

a reduction in their diameter and an increase in energy due to a diamagnetic shift. The shrinkage of the exciton Bohr radius with magnetic field, $a_{\rm B}(B)$, is described by[57]

$$a_{\rm B}(B)=\sqrt{2}a_{\rm B}\left[\sqrt{1+\frac{3}{2}\left(\frac{e^2a_{\rm B}^4B^2}{\hbar^2}\right)}+1\right]^{-1/2},$$

where $a_{\rm B}$ is the zero-field exciton Bohr radius derived by the numerical solution of Eq. (1) and fitting to experimental observations of the diamagnetic shift. As an example, for $a_{\rm B}=10.0$ nm, magnetic fields of $B=5$ T and 10 T shrink $a_{\rm B}(B)$ to about 9.2 nm and 8.0 nm, respectively. Interfacial disorders with shorter lateral lengths of ξ and hence higher energy levels of δE are now active traps that localize excitons with COM momenta that deviate further from $K=0$. Meanwhile, the change to the exciton energy $E_{\rm r}$ can be approached for simplicity by[7,58]

$$E_{{\rm r},B}=E_{{\rm r},0}+\gamma B^2, \tag{4}$$

where γ is the diamagnetic coefficient. Excitons are localized by shorter ξ interfacial disorders when this diamagnetic shift matches δE; this localization of the excitons results in the violation of the $K=0$ selection rule and makes the radiative transition of the dark excitons with $K>0$ possible.[59]

In a low-excitation regime, the total number of generated excitons is $n_{\rm G}$. Among these, some (n_1) are in bright states with degeneracy α_1 and initially accumulate at the interfacial disorders with lateral lengths of ξ_1 (corresponding to an energy of E_1) no smaller than the exciton diameter $D_{\rm ex}$; these contribute to the photoluminescent intensity. The others (n_2) are in dark states with degeneracy α_2, which may transfer to a bright state via magnetic-field-induced localization[7,60] at interfacial disorders with a lateral length of ξ_2 (corresponding to an energy of E_2), such that $\xi_2\le\xi_1$ and $E_2=E_1+\gamma B^2$. Each exciton may be thought of as a complete system, and the exciton–exciton correlations are negligible.[61] While $n_{\rm G}$ is considered to be a constant, n_2 decreases and n_1 increases as the magnetic field strengthens, and the distribution follows

$$n_2/n_1=(\alpha_2/\alpha_1)\,{\rm e}^{-(E_2-E_1)/\Delta E}=\beta\,{\rm e}^{-\gamma B^2/\Delta E},$$
$$n_1+n_2=n_{\rm G},$$

where β is the ratio of the transferable dark states to the bright states at $B=0$ T. For a given radiative efficiency of the bright-state excitons, the field enhancement of the integral PL intensity is given by

$$I_B/I_0=n_1^B/n_1^0=\frac{1+\beta}{1+\beta\,{\rm e}^{-\gamma B^2/\Delta E}}, \tag{5}$$

where n_1^j and I_j represent the number of radiative excitons and the integral PL intensity under zero ($j=0$) and B ($j=B$) magnetic fields. The field enhancement is sensitive to β and $\gamma/\Delta E$. In this regime, the enhancement of the integral PL intensity is a natural result of the field-induced transfer of excitons from the dark states to the bright states, which follows the Urbach rule given in Eq. (3). Here, β and ΔE are the only fitting parameters in the intensity analysis because γ can be derived by fitting the PL energy with Eq. (4); w and hence the FWHM of the lateral-length distribution can be derived using Eq. (3). Furthermore, as the Gaussian distribution starts with a zero lateral length in reality, the mean lateral length of the interfacial disorders $\bar{\xi}$ can be estimated to be $\bar{\xi}\simeq 3w$, if $\exp(-\bar{\xi}^2/2w^2)\sim 10^{-2}$ is taken as the starting point of the $g_{\rm ex}(\xi)$ distribution. As the photoluminescent intensity enhancement arises from the filling of smaller lateral-length interfacial disorders by excitons with non-zero COM momenta, it makes smaller lateral-length interfacial disorders visible via the transfer of excitons from dark to bright states, and may hence serve as a probe that quantifies the Urbach energy and the mean length of the interfacial disorders.

To intuitively demonstrate the effect of $\bar{\xi}$, μ, and β on the magnetic-field enhancement of integral PL intensity, specific examples are illustrated in Fig. 2 with a basic set of parameters $\beta_0=2.0$, $\gamma=0.04$ meV/T^2, $\mu_0=0.05m_0$, and $\bar{\xi}_0=50$ nm. These values are then varied as follows: $1.5\bar{\xi}_0$, $\bar{\xi}_0$, and $0.5\bar{\xi}_0$ in Fig. 2(a); $1.5\mu_0$, μ_0, and $0.5\mu_0$ in Fig. 2(b); and $1.5\beta_0$, β_0, and $0.5\beta_0$ in Fig. 2(c). The (black) solid lines are calculated using the basic set of parameters, and the (red) dashed and (blue) dotted lines are calculated for the specified parameter with multipliers of 1.5 and 0.5, respectively.

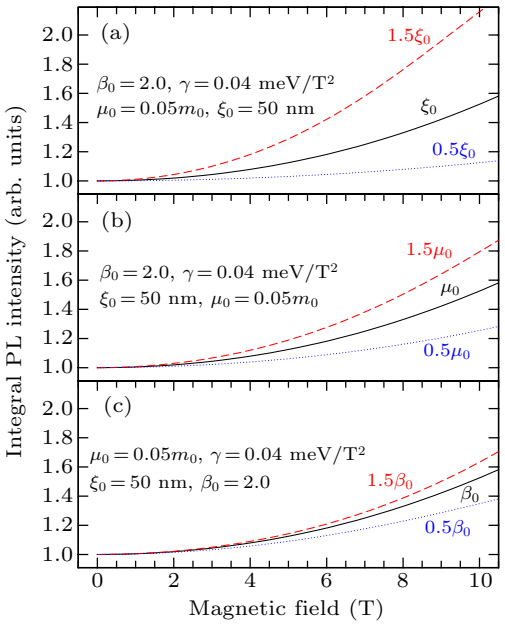


Fig. 2. Effects of $\bar{\xi}$, μ, and β on the magnetic-field enhancement of integral PL intensity. The calculations were performed using Eq. (5) and the following basic parameters: $\beta_0=2.0$, $\gamma=0.04$ meV/T^2, $\mu_0=0.05m_0$, and $\bar{\xi}_0=50$ nm. The parameters were varied for the figure parts as follows: (a) $1.5\bar{\xi}_0$, $\bar{\xi}_0$, $0.5\bar{\xi}_0$; (b) $1.5\mu_0$, μ_0, $0.5\mu_0$; and (c) $1.5\beta_0$, β_0, $0.5\beta_0$. Solid (black) lines were calculated with the basic set of parameters, while dashed (red) and dotted lines (blue) were calculated for the specified parameter with multipliers of 1.5 and 0.5, respectively.

It is clear that at a given magnetic field while changing only one of the three parameters $\bar{\xi}$, μ, and β at a time: (i) a larger value of any one of the three parameters clearly corresponds to a more significant enhancement of the integral PL intensity; (ii) for the same rate of change, $\bar{\xi}$ has the most significant effect on the enhancement, while β has the weakest effect. This is consistent with expectations: from the perspective of the finite-depth square-well approximation, large values of $\bar{\xi}$ and μ correspond to small values of δE, so a relatively low magnetic field is sufficient to provide a matching diamagnetic shift, thereby achieving exciton localization.

Note that though the above theoretical model has not been described previously, a similar treatment was developed for temperature-dependent PL intensity in GaAs,[62] such that $I(T) = I_0/[1 + C\,\mathrm{e}^{-\delta E/k_\mathrm{B}T}]$. This was achieved by taking the electron–hole pair as a complete system and ignoring pair–pair correlations. This approach deals with PL intensity quenching due to the thermal activation of nonradiative, i.e., bright-to-dark transitions and has been widely used for analyzing bulk semiconductors[63–65] and the low-dimensional structures of nanowires, QWs, and SLs,[66–68] together with or in addition to PL energy[69] and linewidth[70] analyses. Analogously, as the model established above deals with the inverse process of integral PL intensity enhancement due to dark-to-bright transitions, it is expected that it will serve as a new efficient vehicle for quantitative magneto-PL analysis of type-I QWs.

3. Experimental details

Two compressively biaxially strained SQW structures of $In_{0.375}Ga_{0.625}N_xAs_{1-x}$/GaAs ($x = 0.012$ and 0.0, denoted by A and B) with a type-I band offset were selected as examples because (i) a previous study of similar SQW samples revealed that the PL features originate in the QW portions with slightly different well thicknesses and are dominated by exciton localization and interfacial effects at temperatures below 100 K,[45,71] and (ii) the material system is important for 1.3–1.55 μm GaAs-based telecom lasers and ultrahigh-efficiency multijunction solar cells. They were grown by molecular beam epitaxy on a (100) GaAs substrate, starting with a 200 nm GaAs buffer layer and a 100 nm $Al_{0.2}Ga_{0.8}As$ layer, followed by a 7 nm thick $In_{0.375}Ga_{0.625}N_xAs_{1-x}$ QW layer sandwiched between two 100 nm GaAs barrier layers, another 100 nm $Al_{0.2}Ga_{0.8}As$ layer, and a 10 nm GaAs cap layer. Part of sample A was treated by post-growth RTA at 750 °C for 30 s and is denoted by A-RTA.

PL measurements were conducted using the 514.5 nm line of an Ar^+-laser as the pumping light and a Fourier transform infrared spectrometer running in continuous-scan mode.[22] The laser beam was loosely focused to a diameter of about 0.5 mm on the sample surface to provide good coverage of the real-space lateral-length Gaussian distribution of interfacial disorders, as illustrated in Fig. 1(b), and the laser power stability was controlled with a laser power controller. A closed-cycle cryostat was used for excitation power-dependent PL measurements at 11 K,[66] and an optical superconducting magnet was employed for magneto-PL measurements at a low temperature of about 4.5 K with the magnetic field perpendicular to the QW plane in the range of 0–10 T.

4. Results and discussion

4.1. Excitation power-dependent PL: amplitude of well-layer thickness fluctuation

Figures 3(a) and 3(b) depict excitation-power-dependent PL spectra in the range of 2–512 mW for the InGaNAs/GaAs SQW samples A and A-RTA. Vertical dashed-dotted lines mark the PL peak positions at an excitation power of 2 mW. Magnifications are applied to the lower-excitation spectra for direct comparison. The PL lineshape is asymmetric, featuring a noticeable low-energy tail at low excitation levels, especially in sample A. This behavior is characteristic of localized state recombination, which has an exponentially distributed density of states[72] and dominates the radiative recombination processes.[73]

The PL spectrum gets stronger and broader as the excitation power rises and can be fitted to two PL components, marked by S and M, for the spectrum of excitation at a power of 32 mW. It has been shown that the splitting of the PL spectrum into two main lines indicates an additional variation in QW mean thickness, here represented by $L_0 \pm \delta$, on a lateral length scale larger than the exciton Bohr radius.[30] At an excitation power of 512 mW, the PL peak uncharacteristically shifts to a lower energy, especially for the sample A-RTA, due to the effect of laser heating. The integral intensity ($\ln I$), energy (E), and linewidth (W) of the two samples, A and A-RTA, manifest similar trends when plotted versus excitation power. The data for the S and M components of sample A are plotted against excitation power using stars and squares, respectively, in Figs. 3(c)–3(e).

The integral PL intensity is reproducible by $I = I_0 P^{k_\mathrm{i}}$ as depicted by the solid line in Fig. 3(c), with $k_\mathrm{i} = 1.01$ for the two PL components. The blueshift manifests a linear characteristic when plotted against $\ln P$, i.e.,

$$P \propto \mathrm{e}^{E/k_\mathrm{e}}, \quad P_2/P_1 \propto \mathrm{e}^{-(E_1-E_2)/k_\mathrm{e}}, \tag{6}$$

which is an exponential distribution similar in form to Eq. (3). A fit to the experimental energy with $E = k_\mathrm{e} \ln P$ is shown in Fig. 3(d), with $k_\mathrm{e} \sim 0.19$ meV and 5.24 meV per unit $\ln P$ (mW) for the S and M components, respectively. The broadening also has a linear relation to $\ln P$, $W = k_\mathrm{w} \ln P$, as shown by the fit plotted in Fig. 3(e), where $k_\mathrm{w} \sim 1.97$ meV and 6.76 meV per unit $\ln P$ (mW) for the S and M components, respectively. Similar phenomena are also observed for sample B.

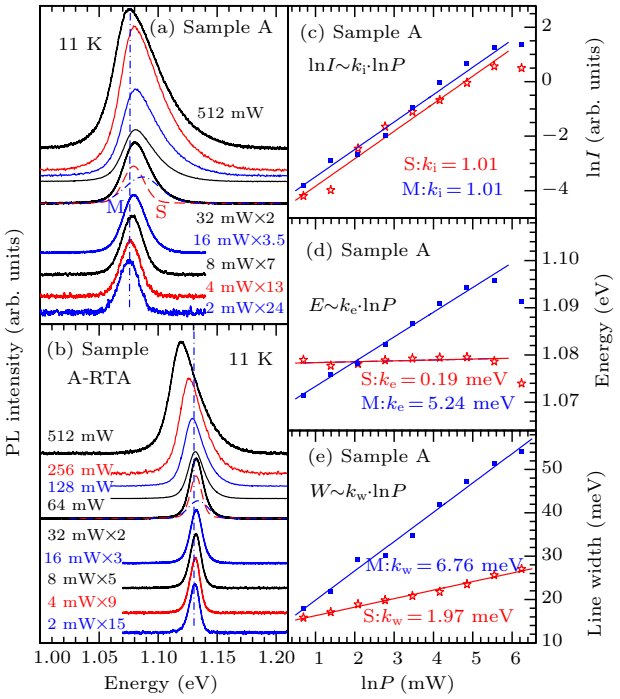


Fig. 3. PL spectra of InGaNAs/GaAs SQW samples A (a) and A-RTA (b) at excitation powers from 2 mW to 512 mW. Vertical dashed-dotted lines mark the peak positions at an excitation power of 2 mW. Magnifications are applied to lower-excitation spectra to make the line shapes visible. Dashed and dashed-dotted lines correspond to two component fits, S and M, at 32 mW. (c) Integral intensity ($\ln I$), (d) energy (E), and (e) linewidth (W) versus excitation power ($\ln P$) for the S and M components of sample A.

It can be seen that, at least in an excitation power range of up to 256 mW, the evolution of integral intensity, energy, and linewidth has a constant rate for each of the PL components and samples. This means that no Mott transition is detectable up to the high-end power of 256 mW,[74] indicating the low-excitation nature of the measurement. The excitonic nature of the PL transitions will be verified by magnetic-field-dependent PL analysis. The results suggest that the well-layer thickness fluctuation follows a Gaussian distribution, and excitation-power-dependent PL analysis can be used to detect such a distribution. As each of the SQW samples contains only one QW layer, the well-layer thickness fluctuation can only exist among different QW regions and appears in the form of interfacial disorders (also known as roughness in, e.g., Refs. [29,30,75]). Given this backdrop, our results provide direct support for the assumption of the height fluctuation of interfacial disorders in transport analyses of GaAs/AlGaAs and InGaAs/InP heterostructures.[11] Coupled with the interfacial disorders shown in Fig. 1(a), one may infer that: (i) the S component shows an inconspicuous blueshift (with $k_e \sim 0.19$ meV per unit $\ln P$ (mW)) and weak broadening (with $k_w \sim 1.97$ meV per unit $\ln P$ (mW)) originating from excitonic transitions in most regions with a QW thickness of around L_0; (ii) the M component originates from excitonic transitions in minor regions where the QW thickness clearly deviates from L_0, which manifests as exciton filling first in the L_+ and gradually in the L_- QW portions as the excitation power increases (and consequently, the nearly 27-fold enlargement of k_e and threefold enlargement of k_w relative to those of the S component); and (iii) the PL peak shows an obvious blueshift as soon as the blueshift of the M component becomes significant, and this situation occurs when the excitation power rises to 32 mW or more.

The amplitude δ of the well-layer thickness fluctuation in different QW regions can be estimated using the blueshift of the M-component to be about 0.55 nm for sample A, 0.15 nm for sample A-RTA, and 0.41 nm for sample B, respectively, with a square well assumption and a solid model method that includes the dilute-N effect.[45] These values are very close to the reported values of 0.45 nm for InGaAs/InP QWs[9] and 0.6 nm for InGaAs/InP SLs.[12] The origin of the well-layer thickness fluctuation is related to indium segregation and nitrogen enhancement. Nonuniform In segregation results in a well-layer thickness fluctuation amplitude of about 0.41 nm in InGaAs/GaAs QW sample B due to a change in the In gradient near the InGaAs/GaAs interface. N incorporation enhances the In segregation and leads to the enlarged amplitude of about 0.55 nm observed in the InGaNAs/GaAs QW sample A.[71] To avoid possible confusion, in the following, the expression interfacial disorders is used uniformly, and the amplitude of the well-layer thickness fluctuation is expressed in terms of the height of the interfacial disorders.

4.2. Magneto-PL: interface flatness

Figures 4(a) and 4(b) show representative magneto-PL spectra of the InGaNAs/GaAs SQW samples A and A-RTA at 4.5 K. The excitation power for the magneto-PL measurement was set to 50 mW (or equivalently, a power density of ~ 25 W/cm^2) to reflect the distribution of the well-layer thickness fluctuation and cover the real-space lateral-length Gaussian distribution of interfacial disorders. The PL spectra become stronger and move to higher energy as the magnetic field increases. The lineshapes are asymmetric and can be fitted using a two-component assumption, as plotted in dashes (I) and a dashed-dotted line (II) for the PL spectra obtained under a zero magnetic field. Note that while the notations S and M were used in the above excitation power-dependent PL analysis, here we use I and II, as it is not relevant whether I corresponds to S or M. The separation between the two PL components is about 12 meV for sample A and narrows due to the RTA treatment to about 1.5 meV for sample A-RTA. This is in accordance with the aforementioned difference in the height δ of the interfacial disorders. Under a zero magnetic field, the PL peak of sample A-RTA appears at 1.13 eV, a higher value than that of sample A at 1.07 eV; its linewidth is, as depicted in Fig. 4(d), about 11.1 meV, narrower than that (17.6 meV) of sample A, as shown in Fig. 4(c). These are the effects of annealing, and the narrowing of the PL peak is also attributed

to the shrinkage of the two-component separation.[45,71]

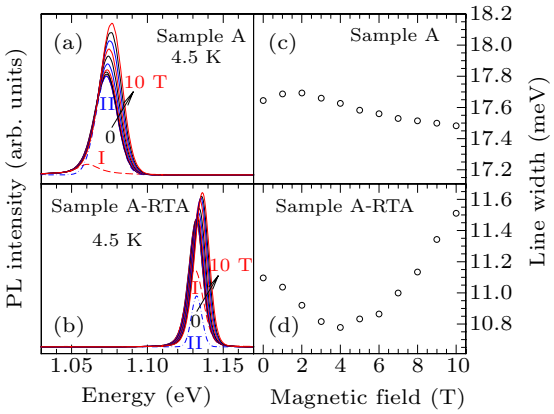


Fig. 4. PL spectra and linewidths of InGaNAs/GaAs SQW samples A (a), (c) and A-RTA (b), (d) in a magnetic field of 0–10 T, excited by a laser power of 50 mW (or equivalently, a power density of ~ 25 W/cm^2). Dashes (I) and dashed-dotted lines (II) in (a) and (b) denote the two-component PL fittings under a zero magnetic field; open circles in (c) and (d) represent the linewidths of the PL peaks.

According to a previous linewidth analysis,[36] the PL linewidth of sample A-RTA, which first narrows by about 0.3 meV and then broadens by 0.7 meV, should be a signature of the coexistence of interfacial disorders with lateral lengths similar to and smaller than the exciton size and the effect of smaller lateral-length interfacial disorders participating in the PL process under a higher magnetic field. The tiny (about 0.2 meV) linewidth narrowing of sample A, on the other hand, might suggest the presence of interfacial disorders with lateral lengths similar to (and larger than) the exciton size.[35] This will be reviewed later as a criterion when the interface flatness is derived.

The energies of the two PL components and the PL peak are depicted in Figs. 5(a) and 5(b) versus magnetic field strength as dots, triangles, and open circles for the two samples A and A-RTA. Fits to the experimental PL energies are made using Eq. (4) and shown as a dashed-dotted line. The derived diamagnetic coefficient γ values from the PL components (I, II) and PL peaks (I+II) are also shown in Figs. 5(a) and 5(b). The $\gamma_{\rm I+II}$ values from the PL peaks are listed in Table 1, where the standard uncertainties are represented by numbers in parentheses. For sample A, $\gamma_{\rm I+II}$ is nearly the same as $\gamma_{\rm II}$, while for sample A-RTA, $\gamma_{\rm I+II}$ is the average of $\gamma_{\rm I}$ and $\gamma_{\rm II}$. This is understandable since, for sample A, PL component II dominates the PL intensity (it is about four times stronger than component I) and energetically nearly coincides with the PL peak, while for sample A-RTA, PL component II plays a similar role to component I, and the PL peak is sandwiched energetically between components I and II, as shown in Fig. 5(b).

It is noteworthy that near the zero field, the fitting deviates from the experimental data. This is because, unlike the excitation- and temperature-dependent PL analyses,[66] here the PL lineshape does not change significantly with the magnetic field strength, making the two-component PL fitting of a slightly asymmetric PL line rather uncertain. For this reason, and in a similar manner to the treatment conducted in a magnetic-field-dependent PL linewidth analysis of the interfacial disorders in $Al_{0.3}Ga_{0.7}As/GaAs/Al_{0.3}Ga_{0.7}As$ QWs,[35] a quantitative comparison will be made based on an analysis of the PL peak as a composite entity, and the results will represent the averaged effect of the filled states in the QW growth direction at a particular excitation power.

Fittings to the experimental PL energies are also made (shown as solid lines in Figs. 5(a) and 5(b)) by numerical calculations based on Eq. (1). The good fits reveal the similar excitonic natures of the two PL components. This, in combination with the composite PL peak, leads to the determination of $E_{\rm b}$, μ, and $D_{\rm ex}$ as listed in Table 1 for the PL peaks of samples A and A-RTA (with the standard uncertainty represented by the numbers in parentheses). These figures provide solid support for the above excitation-power-dependent analysis that the two PL components originate from excitonic transitions in QWs with slightly different layer thicknesses. The RTA process reduces $E_{\rm b}$ and μ while increasing $D_{\rm ex}$ from 26.0±0.3 nm in sample A to 30.2±0.2 nm.

The integral PL intensities are plotted against the magnetic field strength in Figs. 5(c) and 5(d) as dots, triangles, and open circles for the two PL components and the PL peaks of samples A and A-RTA. The maximal field enhancements of the PL peaks occur at $B = 10$ T as $I_{10}/I_0 \approx 1.5$ and 1.2, respectively. The enhancements are nonlinear and are accurately reproduced by Eq. (5) (denoted by solid lines) with the γ derived above and taking β and ΔE as fitting parameters. Based on Eq. (3) and μ, the mean lateral length $\bar{\xi}$ and the FWHM of the lateral-length Gaussian distribution of the interfacial disorders are derived from the PL peaks and also listed in Table 1.

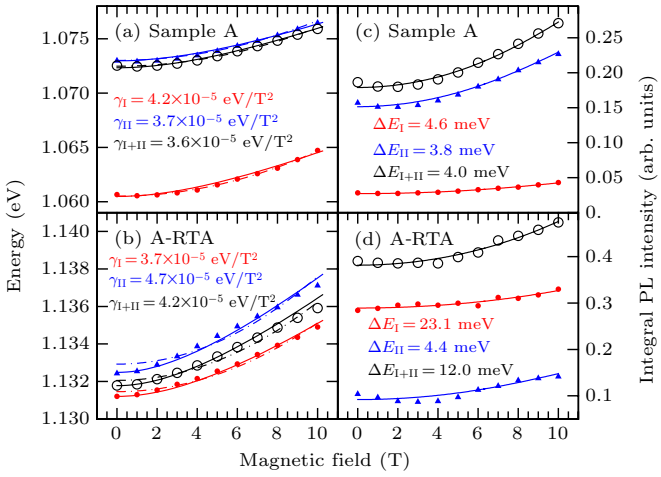


Fig. 5. Energies and intensities of PL components (I, II) and PL peaks (I+II) shown using dots, triangles, and open circles for InGaNAs/GaAs SQW samples A (a), (c) and A-RTA (b), (d) under magnetic fields from 0 to 10 T. The solid lines in (a) and (b) are calculated using Eq. (1), and the dashed-dotted lines are calculated using Eq. (4); the solid lines in (c) and (d) are calculated using Eq. (5).

Table 1. Exciton binding energy E_b (meV), reduced effective mass μ (m_0), diameter D_{ex} (nm), diamagnetic coefficient γ (meV/T^2), enhancement of integral PL intensity I_{10}/I_0 at 10 T, ratio of the transferable dark states to the bright states (at $B = 0$ T) β, interfacial Urbach energy ΔE (meV), mean lateral length $\bar{\xi}$ (nm) and FWHM (nm) of lateral-length Gaussian distribution of interfacial disorders, derived by magneto-PL analysis for the as-grown and post-growth rapid thermally annealed InGaNAs/GaAs SQW samples A and A-RTA, and as-grown InGaAs/GaAs SQW sample B. Numbers in parentheses represent the standard uncertainties of the derived data.

Sample	E_b	μ	D_{ex}	I_{10}/I_0	γ	β	ΔE	$\bar{\xi}$	FWHM
A	9.70(6)	0.0560(5)	26.0(3)	1.5	$3.6(1)\times10^{-2}$	1.4(1)	4.0(3)	55.5(23)	43.6(18)
A-RTA	8.70(6)	0.0480(5)	30.2(2)	1.2	$4.2(2)\times10^{-2}$	2.0(3)	12.1(12)	34.5(17)	27.1(13)
B	8.20(7)	0.0450(5)	32.3(2)	1.6	$5.2(2)\times10^{-2}$	1.1(1)	3.5(3)	66.2(32)	52.0(25)

The values of I_{10}/I_0, β, ΔE, and $\bar{\xi}$ change with post-growth RTA and N incorporation, similarly to E_b, μ, and D_{ex}. Sample A-RTA shows obviously enlarged β and ΔE and reduced I_{10}/I_0 and $\bar{\xi}$. Turning to $\bar{\xi}$ and D_{ex}, while the $\bar{\xi}$ value of sample A is twice as large as the corresponding D_{ex}, that of sample A-RTA is only 0.1 times greater than the corresponding D_{ex}. Both figures are in good agreement with the predicted relation between the exciton diameter and the lateral length of interfacial disorders based on the evolution of the PL linewidth shown in Figs. 4(c) and 4(d). This result therefore supports the correlation between the PL process and interfacial disorders.

To check the universality of the established model and the analytical formula for type-I QWs, magneto-PL analysis was also performed on the as-grown InGaAs/GaAs SQW sample B. The spectra are illustrated in Fig. 6(a), together with representative two-component fittings (I and II) for the spectrum taken at a zero field. The PL peak appears at 1.133 eV at a zero field, i.e., near the peak of sample A-RTA at 1.132 eV. The linewidth of the PL peak as a composite entity is depicted in Fig. 6(b) by open circles. It is only about 7.2 meV under a zero magnetic field, i.e., much narrower than that of sample A-RTA. The linewidth decreases by about 0.5 meV as the magnetic field strength increases, a behavior similar to that of sample A but with a slightly larger magnitude. Again, this might hint at the presence of interfacial disorders with lateral lengths similar to (and larger than) the exciton size,[35] which will be checked shortly.

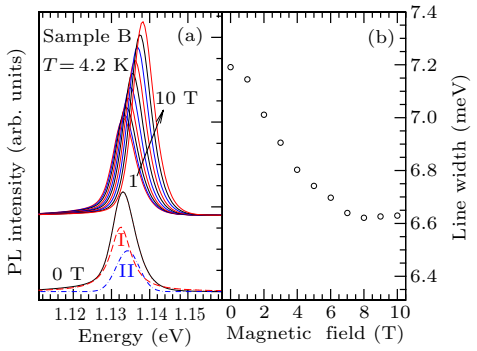


Fig. 6. (a) Magneto-PL spectra with two-component fits (I and II) for the spectrum measured at $B = 0$ T. (b) Linewidth of the PL peak (open circles) of InGaAs/GaAs SQW sample B under magnetic fields ranging from 0 to 10 T, excited with a laser power of 50 mW (or equivalently, a power density of ~ 25 W/cm^2).

The energies of the two PL components and the PL peak are also depicted as dots, triangles, and open circles in Fig. 7(a), which manifest clearly nonlinear evolution and are reproduced using Eq. (1) in solid lines. The derived values of E_b, μ, and D_{ex} are listed in Table 1 for the PL peak, with the standard uncertainties represented by the numbers in parentheses. Fits to Eq. (4), as depicted by dashed-dotted lines give a reasonable match. Using the derived γ's, the integral intensities of the two PL components and the PL peak are also depicted by dots, triangles, and open circles in Fig. 7(b). These are a good fit for the results obtained using Eq. (5), shown as solid lines. The fitting parameters β and ΔE, as well as the $\bar{\xi}$ and FWHM of the lateral-length Gaussian distribution of the interfacial disorders are also listed in Table 1 for the PL peak, together with the maximum enhancement of $I_{10}/I_0 \approx 1.6$ at $B = 10$ T.

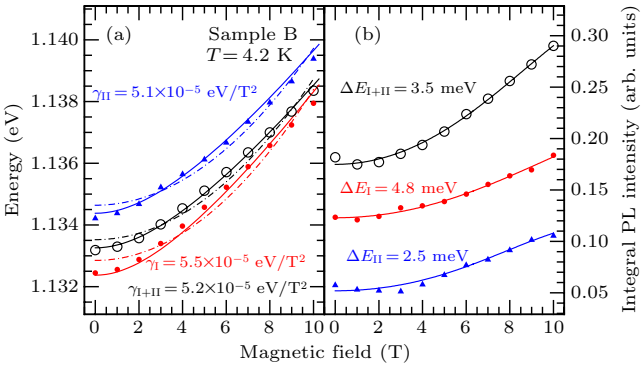


Fig. 7. Energies (a) and integral intensities (b) of two PL components and the PL peak are shown by dots, triangles, and open circles for the InGaAs/GaAs SQW sample B in a magnetic field of 0–10 T. Solid lines in (a) represent the numerical solution of Eq. (1), while dashed-dotted lines were obtained using Eq. (4); solid lines in (b) were calculated using Eq. (5).

The derived $\bar{\xi}$ is similar to that of sample A, i.e., twice as large as the corresponding D_{ex}, again in good agreement with the prediction based on the evolution of the PL linewidth shown in Fig. 6(b). This result supports the correlation between the PL process and the interfacial disorders. Compared to the as-grown InGaNAs/GaAs SQW sample A, the as-grown InGaAs/GaAs SQW sample B manifests smaller E_b, μ, β, and ΔE, and larger D_{ex}, I_{10}/I_0, and $\bar{\xi}$, indicating significant N effects. Considering the field enhancement I_{10}/I_0, it is obvious that: (i) sample B shows the maximal value of 1.6, along with the maximal $\bar{\xi}$ and minimal ΔE values; and (ii) sample A-RTA shows the minimal value of 1.2, along with minimal $\bar{\xi}$ and maximal ΔE values. This reflects the fact that the field enhancement is positively correlated with $\bar{\xi}$ but inversely correlated with ΔE.

The value of $\bar{\xi}$ is similar to the lateral lengths of 26.2 nm for the GaAs/InGaAs interface derived by XSTM[76] and 63 nm for the InGaAs/InP interface derived from transport measurements.[12] The ΔE values fall within the range of reported Urbach energies. For example, an Urbach energy of 8 meV has been measured for (GaIn)(NAs) QWs by analyzing the thermal quenching of PL intensity, specifically considering excitons that are thermally emitted from the localized states to delocalized states above the mobility edge before undergoing nonradiative recombination.[52] Additionally, a value of 20 meV has been determined for InGaN/GaN multiple QWs using biased photocurrent spectroscopy, where the analysis also accounted for fluctuations in well width.[55] These results indicate that the theoretical model correlates the magnetic field enhancement of integral PL intensity with interfacial disorders and effectively reveals the changes in Urbach energy and lateral length distribution of the interfacial disorders from N incorporation to post-growth RTA treatment. The model predicts that, in the application of magnetic-field enhancement to optoelectronic devices,[38,39] smaller Urbach energies ΔE and larger mean lateral lengths $\bar{\xi}$ of interfacial disorders would yield greater enhancement under limited magnetic fields.

4.3. PL enhancement: contribution of energy transfer from excitonic COM motion to electronic degrees of freedom

In reaching a solid conclusion, it is necessary to further examine the rationality of the assumption that the magnetic field causes, via exciton localization to interfacial disorders and breakdown of the $K = 0$ selection rule, the transfer of excitons from dark states to bright states.

As the magnetic field increases, the exciton diameter shrinks. Interfacial disorders with shorter lateral lengths therefore become active in localizing the dark excitons with $K \neq 0$ and kinetic energy $\hbar^2 K^2/2M$ ($M = m^*_{e,\rho} + m^*_{h,\rho}$ is the COM). A momentum-dependent interaction between the COM motion and relative motion is induced, and energy is transferred from the COM motion to the electronic degrees of freedom.[77,78] Consequently, PL intensity enhancement should be observed on the higher-energy side of the PL peak.[61]

For a clear judgment and direct comparison, the magneto-PL spectra of the three InGa(N)As/GaAs SQW samples A, A-RTA, and B are plotted together in Fig. 8 in natural logarithmic intensity, with the shifts of the PL peak and the low- and high-energy edges of the PL peak schematically marked by Δ, Δ_1, and Δ_2, respectively. The vertical bars, horizontal arrows, and dashes are provided to guide the eyes.

The variables Δ, Δ_1, and Δ_2 take values of 3.4 meV, 1.6 meV, and 5.5 meV, respectively, for sample A; 4.2 meV, 3.0 meV, and 5.2 meV, respectively, for sample A-RTA; and 5.2 meV, 4.4 meV, and 6.6 meV, respectively, for sample B. It is clear that regardless of whether the PL linewidth (defined by the FWHM) decreases or increases with the magnetic field, the low-energy edge experiences a smaller blueshift, i.e., $\Delta_1 < \Delta$, while the high-energy edge experiences a more significant blueshift, i.e., $\Delta_2 > \Delta$ and $\Delta_2 \geq \Delta_1 + 2.2$ meV. This means that as the magnetic field increases, in addition to the overall diamagnetic shift of the PL peak with a constant integral intensity, an additional contribution to the higher-energy part beyond the diamagnetic shift appears, which excludes the possible contribution of band tails which would otherwise be seen on the low-energy side. This confirms the prediction above about the magnetic-field-induced localization of $K \neq 0$ excitons and energy transfer from the excitonic COM motion to the electronic degrees of freedom, and hence supports the basic assumption of the magneto-PL intensity model.

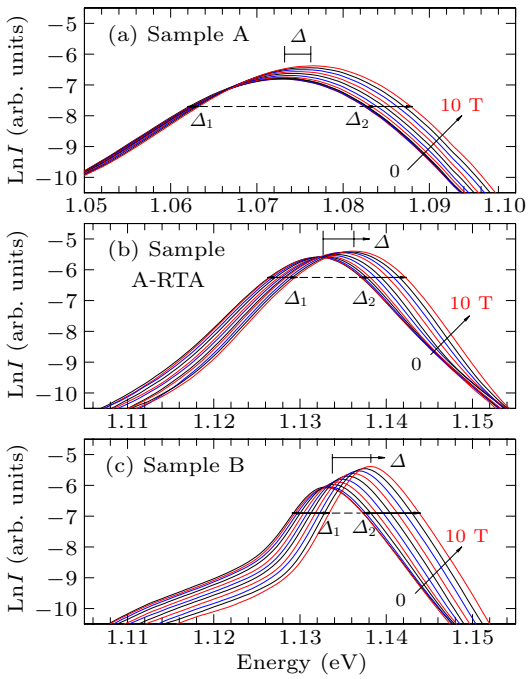


Fig. 8. PL spectra in natural logarithmic intensity for the InGaNAs/GaAs SQW samples A (a), A-RTA (b), and InGaAs/GaAs SQW sample B (c) excited with a laser power of 50 mW (or equivalently, a power density of ~ 25 W/cm^2). Δ_1 and Δ_2 show (marked by horizontal arrows) the shifts of the low- and high-energy edges of the PL peak; vertical bars mark peak positions, and Δ indicates the peak diamagnetic shift in a magnetic field range from 0 to 10 T; horizontal dashes are provided to guide the eyes.

The value of Δ_2 is only slightly different, especially for the two as-grown InGaNAs/GaAs and InGaAs/GaAs SQW samples A and B, for which the enhancements in integral PL intensity I_{10}/I_0 happen to be nearly the same. The $\bar{\xi}$ and ΔE values of the lateral length distribution are more sensitive to RTA but less sensitive to N incorporation: while the $\bar{\xi}$ of the as-grown InGaNAs/GaAs SQW sample A is slightly smaller than that of the InGaAs/GaAs SQW sample B, RTA drastically reduces the $\bar{\xi}$ of the InGaNAs/GaAs SQW sample A-RTA. This is in agreement with previous cross sectional transmission electron microscopy (TEM) analysis of similar

InGa(N)As/GaAs SQW samples, which shows similar nonuniform strain and less sharp interfaces in as-grown samples. Annealing at 750 °C for 30 s obviously improves the uniformity and interface sharpness.[71] The results may suggest that: (i) an indium compositional gradient change and indium segregation are the main origins of the interfacial disorders in InGaAs/GaAs SQWs; the incorporation of N reduces the overall strain and hence $\bar{\xi}$ due to N strain compensation, and (ii) post-growth RTA at 750 °C for 30 s promotes In/N interdiffusion and hence reduces $\bar{\xi}$ and δ.

Before concluding, it would be meaningful to provide a brief overview of the reported research relevant to the magnetic field effects on PL intensity in QWs and SLs. As mentioned above, the integral magneto-PL intensity in QWs has also attracted interest. In a magneto-PL study of type-II $(GaP)_n/(AlP)_n$ short-period SLs, a slight intensity enhancement was observed when an increasing magnetic field was applied parallel to the SL layers, while a dramatic decrease was observed when an increasing perpendicular magnetic field was applied. This anisotropy was explained by assuming a crossover between two closely located conduction bands with different cyclotron masses.[79] In another study, a similar decrease in intensity was observed with an increasing perpendicular magnetic field, but this was considered to be a consequence of bound excitons trapped at the GaP/AlP interface: a defect trapped an excited electron in a conduction band of the AlP layer, and a bound exciton was formed between the trapped electron and a hole in a valence band of the GaP layer.[80] Type-II ultrathin GaAs/AlAs QWs also showed decreasing PL intensity as an increasing perpendicular magnetic field was applied, but the phenomenon was interpreted as the magnetic-field-induced redistribution of indirect excitons between their bright and dark states.[81] In type-I $GaAs/Al_xGa_{1-x}As$ heterostructures, integral PL intensity manifested a striking increase with the applied perpendicular magnetic field, which was explained as a consequence of hole localization caused by an inhomogeneous distribution of background impurities. The contribution from interface roughness was considered negligible here because of the much wider layer thickness of the heterostructures compared to that of the QWs.[82] In $GaAs/Al_{0.28}Ga_{0.72}As$ multiple quantum wells (MQWs) under an excitation power density of ~ 2.5 W/cm^2, asymmetric PL lineshapes were observed and were decomposed into two PL features, of which the low-energy one, associated with the localized energy states, manifested decreasing integral intensity with increasing applied perpendicular magnetic field, while the enhancement of the high-energy feature was considered to be caused by free-exciton transitions.[83] The excitation power density was rather low (only one-tenth of the value used in this study, ~ 25 W/cm^2), which would make band tails apparent; the diamagnetic shifts of the two fitting PL features were not analyzed, and the assumed difference in the nature of the transition (i.e., localized excitons vs. free excitons) was not based on solid experimental analysis. It is obvious that, in general: (i) in type-I QWs and SLs, the integral PL intensity is enhanced as the applied perpendicular magnetic field increases; (ii) in type-II QWs and SLs, the integral PL intensity is reduced as the applied perpendicular magnetic field increases, which is mainly due to the spatial separation of the exciton's electron and hole into different layers; and (iii) although the concept of the magnetic-field-induced redistribution of indirect excitons between bright and dark states was invoked in the type-II QW study, to date, there has been no report correlating the perpendicular magnetic-field-induced enhancement of integral PL intensity in type-I QWs with interface flatness, let alone the derivation of a quantitative theoretical description similar to Eq. (5) presented in this paper.

Meanwhile, it should be valuable to make a brief comparison with the low-temperature absorption of type-I QWs in a similar magnetic field. Experimentally, it has been shown that the enhancement of exciton optical absorption resonance in $In_{0.53}Ga_{0.47}As/InP$ QWs at a temperature of 2 K depends on the strength of the magnetic field applied perpendicular to the QW plane[84] and takes a value of about 50% in a magnetic field range of 0–7 T in a series of QW samples with different QW-layer thicknesses of 6.3 nm, 10.0 nm, and 13.6 nm, though the values of E_b and μ differ from sample to sample.[85] Theoretically, an oscillator strength model[86] was employed to explain the enhancement as a result of magnetic-field-induced shrinkage of well-plane exciton relative-motion wave functions and enhancement of the oscillator strength, and calculations showed that the enhancement in a given range of magnetic field is independent of μ.[84] These results are clearly different from the PL data established in this work, which indicate that the PL enhancement is relevant to E_b and μ, and is different even for an identical QW structure just before and after RTA treatment. The reason for this difference lies in the fact that the low-temperature absorption spectra reveal the free exciton process, and the free-exciton nature can be directly confirmed by the appearance of a negative absorption dip (localized exciton PL) on the low-energy side of the 1e–1h exciton absorption peak in the absorption spectra of similar $In_{1-x}Ga_xAs/InP$ QWs under similar temperature and magnetic field conditions;[46,87] the oscillator strength model is based on the assumption that electron–hole pairs move freely within the QW plane.[84,86] Meanwhile, the low-temperature PL spectrum originates from localized exciton radiative transitions, where electron–hole pairs (excitons) are localized and cannot move freely within the whole QW plane. The oscillator strength model is therefore not applicable and cannot explain the differences in PL enhancement in QW sam-

ples with the same material and structure.

5. Conclusions

To conclude, in this paper, a theoretical model together with an analytical formula is developed to quantitatively account for the evolution of the integral PL intensity in type-I QWs under an external perpendicular magnetic field. The PL transition at low temperature is excitonic and correlates with the QW's interfacial disorders. The lateral length of the interfacial disorders follows a Gaussian distribution and corresponds to an exponential density of states like the Urbach rule. An external magnetic field perpendicular to the QW plane shifts the exciton energy diamagnetically while shrinking its in-plane wave function, so that the excitons in dark states with nonzero COM momentum around $K = 0$ become localized in interfacial disorders with shorter lateral lengths, transfer to bright states, and hence contribute to the PL intensity. Fitting the analytical formula to the experimental integral PL intensity of InGa(N)As/GaAs SQWs allows us to determine the Urbach energy and the lateral-length distribution of the interfacial disorders. The results demonstrate that the model and the formula clarify that the mechanism of the PL intensity enhancement is a joint effect of interfacial disorder-induced exciton localization and a transfer of excitons from dark to bright states. Our results advance the function of magneto-PL experiments from conventional energy and linewidth analyses to also include quantitative integral intensity analysis and provide an avenue for quantitatively characterizing the lateral-length distribution and Urbach energy of the interfacial disorders in type-I QWs. This model may also help improve the performance of magnetic-field-assisted optoelectronic devices.

Acknowledgements

The work was partially supported by the National Natural Science Foundation of China (Grant Nos. 12227901, 12393830, and 12274429) and the STCSM (Grant No. 22QA1410600).

References

[1] Braun W, Kulik L V, Baars T, Bayer M and Forchel A 1998 *Phys. Rev. B* **57** 7196
[2] Lee S, Jo H J, Mathews S, Simon J A, Ronningen T J, Kodati S H, Fink D R, Kim J S, Winslow M, Grein C H, Jones A H, Campbell J C and Krishna S 2019 *Appl. Phys. Lett.* **115** 211601
[3] Wolny P, Turski H, Muziol G, Sawicka M, Smalc-Koziorowska J, Moneta J, Hajdel M, Feduniewicz-Żmuda A, Grzanka S, Kudrawiec R and Skierbiszewski C 2022 *Phys. Rev. Appl.* **19** 014044
[4] Lhuillier E, Ribet-Mohamed I, Rosencher E, Patriarche G, Buffaz A, Berger V and Carras M 2010 *Appl. Phys. Lett.* **96** 061111
[5] Yu C T, Lai W C, Yen C H, Hsu H C and Chang S J 2014 *Opt. Express* **62** A633
[6] Boyle C, Oresick K M, Kirch J D, Flores Y V, Mawst L J and Botez D 2020 *Appl. Phys. Lett.* **117** 051101
[7] Erdmann M, Ropers C, Wenderoth M, Ulbrich R G, Malzer S and Döhler G H 2006 *Phys. Rev. B* **74** 125412
[8] Tabuchi M, Takahashi R, Araki M, Hirayama K, Futakuchi N, Shimogaki Y, Nakano Y and Takeda Y 2000 *Appl. Surf. Sci.* **159–160** 250
[9] Yamakawa I, Oga R, Fujiwara Y, Takeda Y and Nakamura A 2004 *Appl. Phys. Lett.* **84** 4436
[10] Moret N, Oberli D Y, Pelucchi E, Gogneau N, Rudra A and Kapon E 2006 *Appl. Phys. Lett.* **88** 141917
[11] Gold A 1987 *Phys. Rev. B* **35** 723
[12] Pusep Y A, Gozzo G C and LaPierre R R 2008 *Appl. Phys. Lett.* **93** 242104
[13] Zhu L, Shao J, Chen X, Li Y, Zhu L, Qi Z, Lin T, Bai W, Tang X and Chu J 2016 *Phys. Rev. B* **94** 155201
[14] Li J K, Ai L K, Qi M, Xu A H and Wang S M 2018 *Chin. Phys. B* **27** 048101
[15] Pan W, Wang L, Zhang Y, Lei W and Wang S 2019 *Appl. Phys. Lett.* **114** 152102
[16] Huang J Y, Shang L, Ma S F, Han B, Wei G D, Liu Q M, Hao X D, Shan H S and Xu B S 2020 *Chin. Phys. B* **29** 010703
[17] Lu G, Lv Z, Zhang Z, Yang X and Yang T 2021 *Chin. Phys. B* **30** 017802
[18] Huang J, Zhuo H C Z, Wang J, Li S, Ding K, Ni H, Niu Z, Jiang D, Dou X and Sun B 2021 *Chin. Phys. B* **30** 097805
[19] Zhu L, Liu S, Shao J, Chen X, Liu F, Hu Z and Chu J 2023 *Chin. Phys. Lett.* **40** 077503
[20] Ma S F, Li L, Kong Q B, Xu Y, Liu Q M, Zhang S, Zhang X S, Han B, Qiu B C, Xu B S and Hao X D 2023 *Chin. Phys. B* **32** 037801
[21] Li S, Shao P, Liang X, Chen S, Li Z, Su X, Tao T, Xie Z, Liu B, Khan M A, Wang L, Lin T T, Hirayama H, Zhang R and Wang K 2024 *Chin. Phys. B* **33** 126801
[22] Shao J, Chen X, Wang M and Lu W 2025 *Acta Phys. Sin.* **74** 017801 (in Chinese)
[23] Shao J, Lu W, Lü X, Yue F, Li Z, Guo S and Chu J 2006 *Rev. Sci. Instrum.* **77** 063104
[24] Shao J, Chen L, Lü X, Lu W, He L, Guo S and Chu J 2009 *Appl. Phys. Lett.* **95** 041908
[25] Shao J, Chen L, Lu W, Lu X, Zhu L, Guo S, He L and Chu J 2010 *Appl. Phys. Lett.* **96** 121915
[26] Chen X, Zhu L and Shao J 2019 *Rev. Sci. Instrum.* **90** 093106
[27] Chen X, Zhu L, Zhang Y, Zhang F, Wang S and Shao J 2021 *Phys. Rev. Appl.* **15** 044007
[28] Chen X and Shao J 2024 *Rev. Sci. Instrum.* **95** 123906
[29] Grousson R, Voliotis V, Grandjean N, Massies J, Leroux M and Deparis C 1997 *Phys. Rev. B* **55** 5253
[30] Jahn U, Kwok S H, Ramsteiner M, Hey R, Grahn H T and Runge E 1996 *Phys. Rev. B* **54** 2733
[31] Zhang X C, Chang S K, Nurmikko A V, Kolodziejski L A, Gunshor R L and Datta S 1985 *Phys. Rev. B* **31** 4056
[32] Zhou W G, Jiang D W, Shang X J, Wu D H, Chang F R, Jiang J K, Li N, Lin F Q, Chen W Q, Hao H Y, Liu X L, Tan P H, Wang G W, Xu Y Q and Niu Z C 2023 *Chin. Phys. B* **32** 088501
[33] Sugawara M, Okazaki N, Fujii T and Yamazaki S 1993 *Phys. Rev. B* **48** 8102
[34] Shao J, Winterhoff R, Dörnen A, Baars E and Chu J 2003 *Phys. Rev. B* **68** 165327
[35] Bansal B, Hayne M, Arora B M and Moshchalkov V V 2007 *Appl. Phys. Lett.* **91** 251108
[36] Chen X, Xu Z, Zhou Y, Zhu L, Chen J and Shao J 2020 *Appl. Phys. Lett.* **117** 081104
[37] Haldar S, Dixit V K, Vashisht G, Porwal S and Sharma T K 2018 *J. Appl. Phys.* **124** 055704
[38] Wade A, Fedorov G, Smirnov D, Kumar S, Williams B S, Hu Q and Reno J L 2009 *Nat. Photon.* **3** 41
[39] Maëro S, Louis-Anne de Vaulchier, Guldner Y, Deutsch C, Krall M, Zederbauer T, Strasser G and Unterrainer K 2013 *Appl. Phys. Lett.* **103** 051116
[40] Damen T C, Vina L, Cunningham J E and Shah J 1991 *Phys. Rev. Lett.* **67** 3432
[41] Damen T C, Shah J, Oberli D Y, Chemla D S, Cunningham J E and Kuo J M 1990 *Phys. Rev. B* **42** 7434
[42] Kurdyubov A S, Trifonov A V, Gerlovin I Y, Gribakin B F, Grigoryev P S, Mikhailov A V, Ignatiev I V, Efimov Y P, Eliseev S A, Lovtcius V A, Aßmann M, Bayer M and Kavokin A V 2021 *Phys. Rev. B* **104** 035414

[43] Reischle M, Beirne G J, Roßbach R, Jetter M and Michler P 2008 *Phys. Rev. Lett.* **101** 146402
[44] Chang K and Peeters F M 2001 *Phys. Rev. B* **63** 153307
[45] Shao J, Qi Z, Zhao H, Zhu L, Song Y, Chen X, Zha F X, Guo S and Wang S M 2015 *J. Appl. Phys.* **118** 165305
[46] Shao J, Dörnen A, Baars E, Härle V, Scholz F, Guo S and Chu J 2003 *J. Appl. Phys.* **93** 951
[47] Wager J F 2017 *AIP Adv.* **7** 125321
[48] Urbach F 1953 *Phys. Rev.* **92** 1324
[49] Eliseev P G, Perlin P, Lee J and Osiński M 1997 *Appl. Phys. Lett.* **71** 569
[50] Kaschner A, Lüttgert T, Born H, Hoffmann A, Egorov A Y and Riechert H 2001 *Appl. Phys. Lett.* **78** 1391
[51] Pan Y, Inam F, Zhang M and Drabold D A 2008 *Phys. Rev. Lett.* **100** 206403
[52] Rubel O, Baranovskii S D, Hantke K, Rühle W W, Thomas P, Volz K and Stolz W 2006 *Phys. Stat. Sol. (c)* **3** 2481
[53] Bleuse J, Perret S, Curé Y, Grenet L, André R and Mariette H 2020 *Phys. Rev. B* **102** 195205
[54] Kaiser C, Sandberg O J, Zarrabi N, Li W, Meredith P and Armin A 2021 *Nat. Commun.* **12** 3988
[55] Piccardo M, Li C K, Wu Y R, Speck J S, Bonef B, Farrell R M, Filoche M, Martinelli L, Peretti J and Weisbuch C 2017 *Phys. Rev. B* **95** 144205
[56] Kammerer C, Cassabois G, Voisin C, Delalande C, Roussignol P and Gérard J M 2001 *Phys. Rev. Lett.* **87** 207401
[57] Stępnicki P, Piętka B, Morier-Genoud F, Deveaud B and Matuszewski M 2015 *Phys. Rev. B* **91** 195302
[58] Patricio M A T, Villegas-Lelovsky L, de Oliveira E R C, Marques G E, LaPierre R R, Toropov A I and Pusep Y A 2023 *Phys. Rev. B* **108** 035416
[59] Hohenester U, Goldoni G and Molinari E 2005 *Phys. Rev. Lett.* **95** 216802
[60] Schaller R D, Crooker S A, Bussian D A, Pietryga J M, Joo J and Klimov V I 2010 *Phys. Rev. Lett.* **105** 067403
[61] Schnabel R F, Zimmermann R, Bimberg D, Nickel H, Losch R and Schlapp W 1992 *Phys. Rev. B* **46** 9873
[62] Bimberg D, Sondergeld M and Grobe E 1971 *Phys. Rev. B* **4** 3451
[63] Callsen G, Wagner M R, Kure T, Reparaz J S, Bugler M, Brunnmeier J, Nenstiel C, Hoffmann A, Hoffmann M, Tweedie J, Bryan Z, Aygun S, Kirste R, Collazo R and Sitar Z 2012 *Phys. Rev. B* **86** 075207
[64] Chen X, Wu X, Yue L, Zhu L, Pan W, Qi Z, Wang S and Shao J 2017 *Appl. Phys. Lett.* **110** 051903
[65] Herklotz F, Lavrov E V, Melnikov V V, Galazka Z and Agekyan V F 2023 *Phys. Rev. B* **108** 205204
[66] Shao J, Lu W, Tsen G K O, Guo S and Dell J M 2012 *J. Appl. Phys.* **112** 063512
[67] Chen X, Zhou Y, Zhu L, Qi Z, Xu Q, Xu Z, Guo S, Chen J, He L and Shao J 2014 *Jpn. J. Appl. Phys.* **53** 082201
[68] Chen X, Zhuang Q, Alradhi H, Jin Z M, Zhu L, Chen X and Shao J 2017 *Nano Lett.* **17** 1545
[69] Varshni Y 1967 *Physica* **34** 149
[70] Qiao H, Abel K A, van Veggel F C J M and Young J F 2010 *Phys. Rev. B* **82** 165435
[71] Zhao H, Wang S M, Zhao Q X, Lai Z H, Sadeghi M and Larsson A 2008 *Semicond. Sci. Technol.* **23** 125002
[72] Ishikawa F, Álvaro Guzmán, Brandt O, Trampert A and Ploog K H 2008 *J. Appl. Phys.* **104** 115302
[73] Hong Y G, Nishikawa A and Tu C W 2003 *Appl. Phys. Lett.* **83** 5446
[74] Kappei L, Szczytko J, Morier-Genoud F and Deveaud B 2005 *Phys. Rev. B* **94** 147403
[75] Semtsiv M P, Flores Y, Chashnikova M, Monastyrskyi G and Masselink W T 2012 *Appl. Phys. Lett.* **100** 163502
[76] Chao K J, Liu N, Shih C K, Gotthold D W and Streetman B G 1999 *Appl. Phys. Lett.* **75** 1703
[77] Schmelcher P and Cederbaum L S 1995 *Phys. Rev. Lett.* **74** 662
[78] Getter A and Perakis I E 1999 *Phys. Rev. B* **60** 16027
[79] Uchida K, Miura N, Kitamura J and Kukimoto H 1996 *Phys. Rev. B* **53** 4809
[80] Kobayashi Y, Kouzu K and Kamimura H 1999 *Solid State Commun.* **109** 583
[81] Shamirzaev T S, Debus J, Yakovlev D R, Glazov M M, Ivchenko E L and Bayer M 2016 *Phys. Rev. B* **94** 045411
[82] Zhao Q X, Monemar B, Holtz P O, Lundström T, Sundaram M, Merz J L and Gossard A C 1994 *Phys. Rev. B* **50** 7514
[83] Haldar S, Dixit V K, Vashisht G, Porwal S and Sharma T K 2017 *J. Phys. D: Appl. Phys.* **50** 335107
[84] Sugawara M 1992 *Phys. Rev. B* **45** 11423
[85] Sugawara M, Okazaki N, Fujii T and Yamazaki S 1993 *Phys. Rev. B* **48** 8848
[86] Ferreira R, Soucail B, Voisin P and Bastard G 1990 *Phys. Rev. B* **42** 11404
[87] Shao J, Haase D, Dörnen A, Härle V and Scholz F 2000 *J. Appl. Phys.* **87** 4303